IL NUOVO CIMENTO Vol. 29 C, N. 6 Novembre-Dicembre 2006
DOI 10.1393/ncc/i2006-10021-3

Application of the K-edge X-ray technique to map pigments of art paintings: Preliminary results

P. Baldelli([1]), L. Bonizzoni([2]), M. Gambaccini([1]), M. Gargano([2]), L. Ludwig([2]), M. Milazzo([2]), L. Pasetti([1]), F. Petrucci([1]), F. Prino([4]), L. Ramello([3])([4]) and M. Scotti([1])

([1]) *Dipartimento di Fisica dell'Università and INFN, Sezione di Ferrara - Ferrara, Italy*
([2]) *Istituto di Fisica Generale Applicata dell'Università and INFN, Sezione di Milano Milano, Italy*
([3]) *Dipartimento di Scienze e Tecnologie Avanzate dell'Università del Piemonte Orientale Torino, Italy*
([4]) *INFN, Sezione di Torino - Torino, Italy*

(ricevuto il 21 Giugno 2006; revisionato il 10 Ottobre 2006; approvato il 20 Ottobre 2006)

Summary. — The topographic map of pigments of paintings is a powerful tool for detecting execution techniques, *pentimenti* and underpaintings hidden to usual imaging diagnostics. Neutron activation autoradiography has provided significant results in few and very important instances. Because of the cost of the nuclear reactor facility needed for a complete painting examination, new technologies to obtain the topographic map of pigments are desirable. Dual-energy radiography can pursue the same goal by tuning the energy gap on the K-absorption edge of interesting elements. The proposed technique is based on the use of quasi-monochromatic beams, with energy below and above the threshold of K absorption of the considered element. In this way two final images are obtained showing the distribution of the specific element and the distribution of all other materials. Preliminary results have been obtained by using samples containing cadmium.

PACS 07.85.-m – X- and gamma-ray instruments.

1. – Introduction

XRF and PIXE are well-known methods of obtaining elemental composition of pigments in paintings. These applications allow the identification of many materials in a completely non-invasive fashion. They have largely developed art-history knowledge in many relevant examples: from the chronology of azurite and ultramarine in illuminated codes [1] to the evolution of colour palette in Caravaggio masterpieces [2], to the composition of various parts of the Corona Ferrea [3], to the identification of pigments in the wood painting by Leonardo da Vinci "Madonna dei fusi" [4]. Now interest among art historians and restorers is growing for mapping elements in a painting, rather than

sampling. The topographic map of a pigment, obtained from the distribution of an indicative element, is indeed a powerful tool for detecting execution technique, *pentimenti* and underpaintings often hidden to usual imaging diagnostics. In fact, some underpaintings are not detectable neither by X-ray radiograph because they are made by low-Z elements like carbon nor by IR reflectography because the paint layer above is too thick. The topographic map of a pigment, reached in few and very important instances by neutron activation autoradiography [5] seems to be limited by the possibility of exposing the whole artwork to the thermal neutron irradiation facility of a nuclear reactor. Because of the cost of a nuclear reactor facility and of the time required to perform the examination, a development of new technologies to obtain the map of pigments is desirable. For this purpose we are investigating the use of a quasi-monochromatic tuneable and compact X-ray source for K-edge subtraction technique application on paintings. This technique was first used in the radiological environment for blood vessel imaging [6, 7]. The K-edge technique takes advantage of the sharp rise of the X-ray absorption coefficient of a suitable contrast agent. Two monochromatic X-ray beams with energies bracketing the K-edge energy are used to acquire two images of coronaries after the injection of the contrast agent. There are two ways to process the so-acquired images. The first is the logarithmic subtraction of the two images: the signals due to the soft tissue and bone thickness variations are strongly suppressed after the logarithmic subtraction of the two energy images, and the signal arising by the distribution of the contrast agent is strongly enhanced in the final image. The two images can also be processed by the dual-energy method proposed by Lehmann [8]. This technique allows decomposing the sample in two different base materials, so that the contrast agent can be distinguished from all other materials. After image processing, two images are obtained: the first is the contrast medium concentration map while the second is the image of all other materials.

By transferring this technique from a medical environment to the art environment, it would be possible to recognize, based on its K-edge absorption, a particular element. In addition, applying Lehmann's algorithm for image analysis makes it possible to map the distribution of the element on a region of the painting.

Most pigments contain heavy elements like copper (azurite, red enamel, green enamel, malachite green viridian green, verdigris), zinc (zinc white, cadmium yellow, cobalt green, zinc green), arsenic (realgar, cobalt violet, viridian green), strontium (strontium yellow), cadmium (cadmium orange, cadmium yellow, cadmium red, cadmium green, yellow enamel) which have a K-edge in the 9–28 keV energy range. In principle, using quasi-monochromatic X-rays with energy just above and below the K-edge of a specific element, it would be possible to obtain the distribution of that element in the painting. In this work preliminary results of measurements carried out to test the potentiality and the applicability of this technique are presented. Tests have been carried out using two different cadmium samples (K-edge 26.71 keV): a cadmium metal sheet and a painting mixture of cadmium red pigment.

2. – Materials and methods

2˙1. *Description of the X-ray source.* – Quasi-monochromatic X-rays can be obtained with a standard X-ray tube by using Bragg diffraction on mosaic crystals. Mosaic crystals are considered good candidates for monochromator design because of their high reflectivity [9]. A mosaic crystal is formed by a large number of perfect microcrystallites which act like an aggregate of independently scattering ideal crystals. The angular distribution of the normals to the lattice planes of the microcrystallites is approximately

Gaussian (the standard deviation for graphite mosaic crystals ranged between 0.1° and 0.5°). Quasi-monochromatic beam with a given energy can be produced by choosing a suitable angle between the source and the crystal in accordance with the Bragg law:

$$2d \sin \theta_{\mathrm{B}} = n\lambda \,, \tag{1}$$

where d is the distance between the lattice planes, λ is the wavelength of the beam and n is the diffraction order. By expressing λ as a function of the energy E, the Bragg law becomes

$$2d \sin \theta_{\mathrm{B}} = n \frac{1.24}{E} \,, \tag{2}$$

where E is in keV, and d is in nm.The quasi-monochromatic system used in this experiment has been developed for mammography application [10]. The system has been modified in order to reach energy higher than the cadmium K-edge energy (26.7 keV). The schematic representation of the prototype system is reported in fig. 1. The photon source consists of an X-ray tube manufactured by Gilardoni (Mandello del Lario, Italy) with tungsten anode, 2 mm Be window, a nominal focal spot size of 1×2 mm^2, a maximum peak voltage of 60 kV and a maximum current of 600 mA. The tube is mounted on a motorized goniometer that can rotate between $2\theta = 16.64°$ and $2\theta = 7.56°$ corresponding to the energy range of 16–28 keV. A primary collimation system consisting of two lead slits is placed downstream of the X-ray tube so as to match the incident X-ray beam divergence to the crystal monochromator dimensions. The bremsstrahlung beam is monochromatized via Bragg diffraction by a highly oriented pyrolytic graphite mosaic crystal (HOPG), supplied by Optigraph (Optigraph Ltd, Moscow, Russia) 60×28 mm^2 wide, 1 mm thick with a measured mosaic spread of 0.28°. The crystal is mounted on another isocentric motorized goniometer (Microcontrole SR50CC) placed at 15 cm from the X-ray tube focal spot that can rotate between $\theta = 0°$ and $\theta = 8.32°$. This set-up provides a diffracted beam always perpendicular to the imaging plane independently of the tuned X-ray energy. At the exit of the crystal, the diffracted beam is collimated by three lead slits placed at 10, 25 and 35 cm from the crystal, respectively. The first two have fixed exit and the last one has a manually adjustable width which ranges from 5 mm to 20 mm. After the third collimator at 45 cm from the crystal and at 64 cm from the X-ray tube focal spot the 2D detector is mounted on a motorized scanning system (Minimotor 3557K024CS) with an adjustable speed ranging between 20 and 100 mm/s. The X-ray tube, the crystal and the scanning system are connected to a multi axis motion controller unit (Microcontrole MM4006). This unit and the X-ray tube generator are interfaced to a personal computer which controls the whole image acquisition process.

2˙2. *Detection systems.* – Two detectors have been used to acquire images and diffracted X-ray spectra used for image acquisition.

The first detector is the RadEye2 [11] module packaged together with a Gd_2O_2S scintillator (Kodak Min-R Medium) in direct contact with the sensor, and a thin graphite window to protect the array. The large (49.2 mm by 49.3 mm) active area consists of a 1024 by 1024 matrix of silicon photodiodes with 48 μm pitch. The RadEye2 is optimized to detect X-rays and other energetic radiation in the 10 keV to 50 keV range. An evaluation board is designed as a test adapter to connect the detector to a data acquisition board from National Instruments. With this connection, the detector functions can be

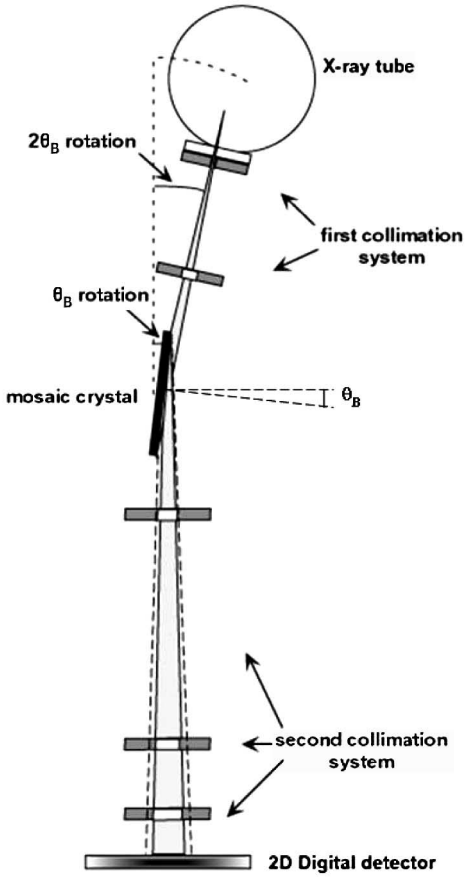

Fig. 1. – Schematic representation of the quasi-monochromatic system.

controlled from a simple LabView program, and images can be acquired and saved on a PC.

Since the X-ray diffracted beam is laminar only a rectangular part (49.2 mm×14 mm) of the detector is used for image acquisition.

A CdTe detector (Amptek mod.XR-100T) with a surface area of 3×3 mm^2 and a beryllium entrance window 1 mm thick, connected to a multichannel analyzer, has been employed to measure diffracted X-ray spectra used for image acquisition.

2˙3. *Samples*. – Preliminary measurements have been applied on two kinds of samples. The first is a uniform sample and consists of a 127 μm thick Cd sheet. The second sample is cadmium red powder (CdS) diluted in Dammar gum and trementine essence, spread on a Mylar sheet. This sample has been formerly analyzed by XRF, in order to confirm the presence of the target element in the painting material.

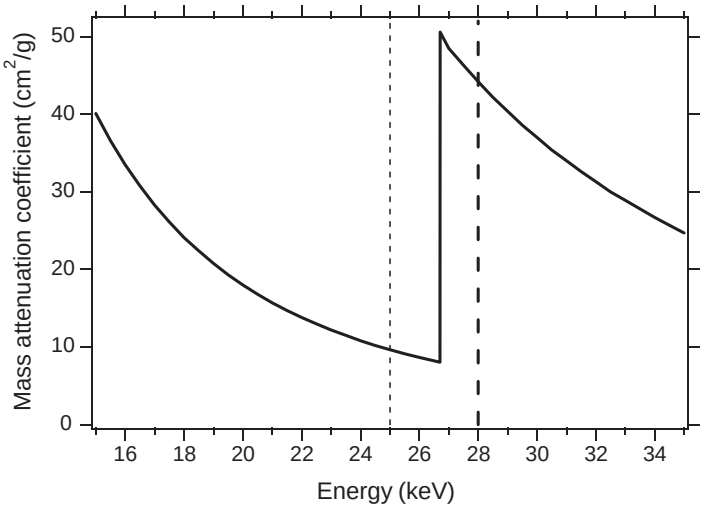

Fig. 2. – Mass attenuation coefficient of the cadmium. The two dashed lines represent the energies used for images acquisition.

3. – Images acquisition and processing

3˙1. *First sample*. – Four images of the uniform sample described above have been acquired in the 25–28 keV energy range in order to verify the shift of the K-edge absorption on images when the energy increases. The sample has been imaged by setting a tube loading of 50 kV in order to maximize the flux and avoiding the second diffraction order from the diffracted beam [12] in accordance with eq. (2). Indeed if the Bragg angle is set to a value corresponding to the generic energy E, Bragg formula for mosaic crystals

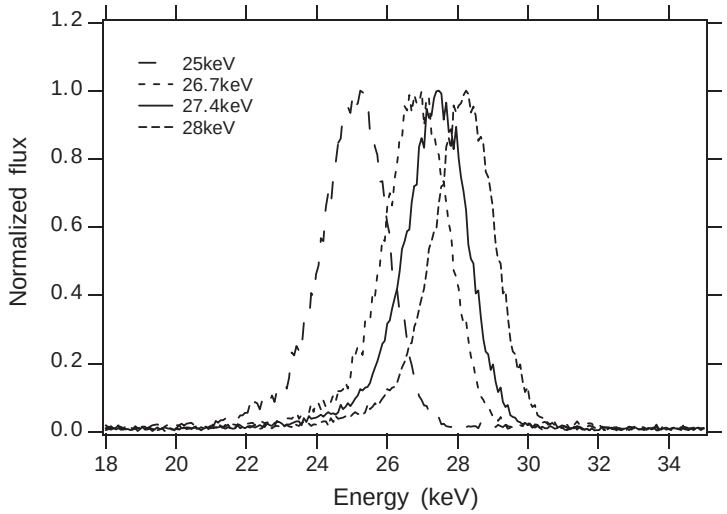

Fig. 3. – Diffracted X-ray spectra acquired at 25, 26.7, 27.4 and 28 keV acquired with the CdTe detector.

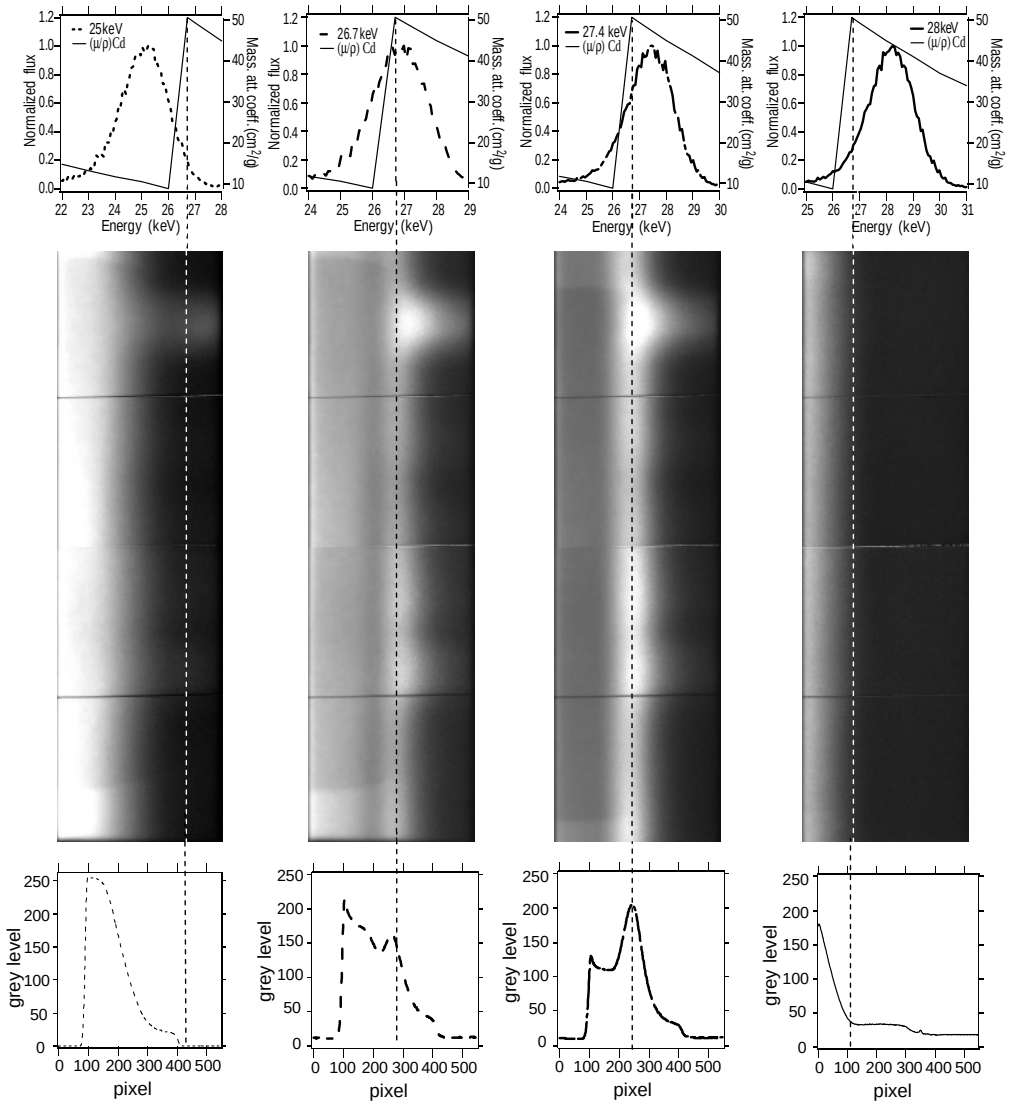

Fig. 4. – Diffracted X-ray beams spectra acquired at energies of 25 keV, 26.7 keV, 27.4 keV and 28 keV are reported in the top. In the middle the corresponding images are reported, while in the bottom the profiles measured on the images are shown. The darker levels mean lower photon-flux.

is satisfied also by photons having energy $2E$, $3E$, $4E$ etc., according to the diffraction order $n = 2, 3, 4$ etc. The maximum kVp value of the incident beam should not be over twice the selected energy measured in keV.

After the acquisition, images have to be processed for the flat-field corrections to remove artefacts caused by variations in the pixel-to-pixel sensitivity of the detector and by the non-uniformity of the radiation field. For each corrected image a profile of intensity as a function of the position has been plotted.

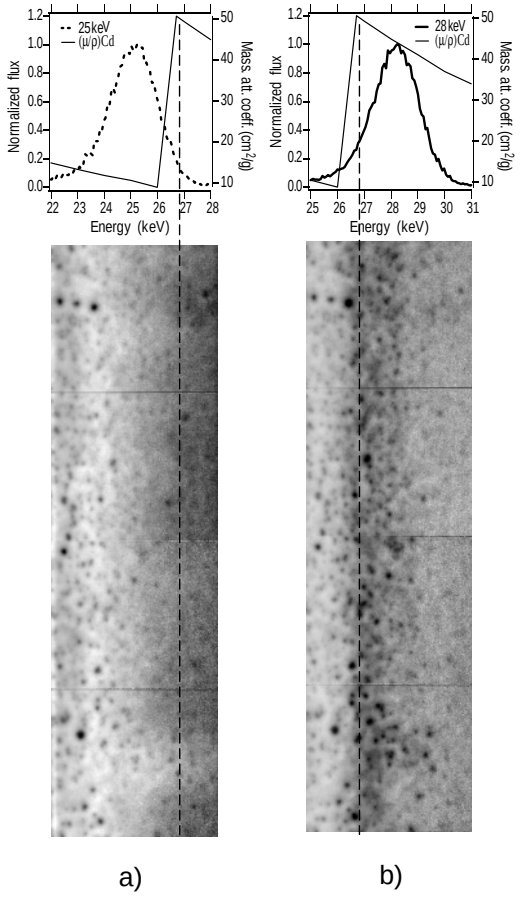

Fig. 5. – a) Energy distribution of the diffracted beam measured at 25 keV (top) and the corresponding image acquired at 25 keV (bottom); b) energy distribution of the diffracted beam measured at 28 keV (top) and the corresponding image acquired at 28 keV (bottom).

3˙2. *Second sample.* – The K-edge subtraction technique has been applied on the second kind of sample. For monochromatic X-rays, the signal in the raw images is proportional to the number of photons impinging on the detector after the transmission through the object

$$N(E_{\pm}) = N_0(E_{\pm}) \cdot \exp\left[-\sum_i \left[\frac{\mu}{\rho}(E_{\pm})\right]_i \cdot (\rho t)_i\right] , \tag{3}$$

where N_0 is the mean number of incident photons per unit area, E_+ and E_- are the two energies that bracket the K-edge discontinuity, (μ/ρ) and ρ are the mass attenuation coefficient and the density of materials, respectively, and t is the transmitted path length. The subscript i denotes the different materials that compose the sample (cadmium, Dammar gum, trementine and Mylar). It is possible to calculate a "cadmium image" from the two energy images by using Lehmann's algorithm [13, 8] which allows

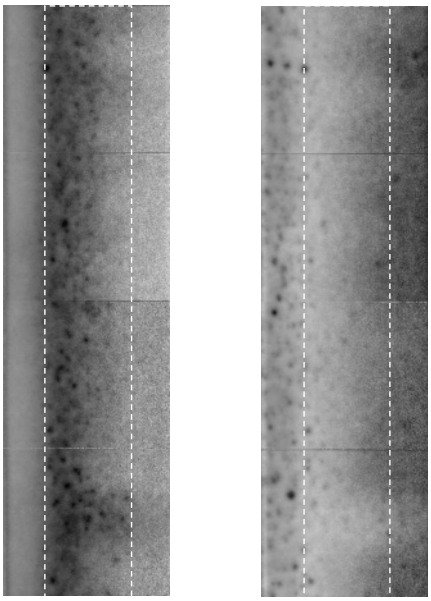

Fig. 6. – Images processed for the dual-energy algorithm, a) "cadmium image" shows the distribution of the cadmium element on the sample, b) "Mylar image" shows the distribution of all the other materials on the sample.

decomposing the sample in two base materials. This method considers the linear attenuation coefficient of two base materials to form an orthogonal coordinate system where each point represents a certain mixture of the two base materials. We chose as base materials cadmium and Mylar and in this way the element cadmium can be distinguished from the fictitious element mylar which comprises all other materials (Dammar gum, trementine and Mylar). If the beams are assumed to be monochromatic, eq. (3) can be rewritten as a function of base materials as

$$\ln \frac{N_0}{N}(E_\pm) = \left[\frac{\mu}{\rho}(E_\pm)\right]_{\mathrm{Cd}} \cdot (\rho t)_{\mathrm{Cd}} + \left[\frac{\mu}{\rho}(E_\pm)\right]_{\mathrm{Mylar}} \cdot (\rho t)_{\mathrm{Mylar}} \tag{4}$$

where $(\mu/\rho)_{\mathrm{Cd}}$ and $(\mu/\rho)_{\mathrm{Mylar}}$ are mass attenuation coefficients of cadmium and Mylar at the energies of interest, $(\rho t)_{\mathrm{Cd}}$ is the mass density of cadmium and $(\rho t)_{\mathrm{Mylar}}$ is the Mylar equivalent mass density of all other materials (in g/cm^2). The quantities (μ/ρ) at the two energies E_+ and E_- are known, while the mass densities ρt of cadmium and Mylar are unknown quantities independent of beam energies. These latter quantities can be calculated, pixel by pixel, by solving the two logarithmic transmissions in eq. (4). In this way two final images are obtained from the raw images: the *cadmium image*, that is a map of the cadmium distribution and the *Mylar image*, that is the map of all other

TABLE I. – *Mass attenuation coefficients of cadmium and Mylar used for the application of the K-edge algorithm.*

Energy (keV)	$(\mu/\rho)_{\mathrm{Cd}}$ ($\mathrm{cm^2 g^{-1}}$)	$(\mu/\rho)_{\mathrm{Mylar}}$ ($\mathrm{cm^2 g^{-1}}$)
25	10.5	0.387
28	44.9	0.328

materials. They are given by

$$(\rho t)_{\mathrm{Cd}} = \frac{\left[\frac{\mu}{\rho}(E_-)\right]_{\mathrm{Mylar}} \cdot \ln \frac{N_0}{N}(E_+) - \left[\frac{\mu}{\rho}(E_+)\right]_{\mathrm{Mylar}} \cdot \ln \frac{N_0}{N}(E_-)}{K_0}, \tag{5}$$

$$(\rho t)_{\mathrm{Mylar}} = \frac{\left[\frac{\mu}{\rho}(E_+)\right]_{\mathrm{Cd}} \cdot \ln \frac{N_0}{N}(E_-) - \left[\frac{\mu}{\rho}(E_-)\right]_{\mathrm{Cd}} \cdot \ln \frac{N_0}{N}(E_+)}{K_0} \tag{6}$$

with

$$K_0 = \left[\frac{\mu}{\rho}(E_-)\right]_{\mathrm{Mylar}} \cdot \left[\frac{\mu}{\rho}(E_+)\right]_{\mathrm{Cd}} - \left[\frac{\mu}{\rho}(E_+)\right]_{\mathrm{Mylar}} \cdot \left[\frac{\mu}{\rho}(E_-)\right]_{\mathrm{Cd}}. \tag{7}$$

In order to optimize the analysis the choice of the energy of the monochromatic beams which have to be used is very important. In fact, to make the most of the different absorption in the K-edge energy range, the quasi-monochromatic beam with energy just below and above the K-edge energy should be used. Since quasi-monochromatic beams have an energy resolution of about 7.5% (FWHM), in order to reduce the overlapping of the two spectra which causes artefacts on image, a proper spectral separation is required. Taking into account this two conflicting requirements, images of the sample have been acquired at 25 keV and 28 keV. Attenuation coefficients for the base materials have been calculated via the XCOM program [14]. Figure 2 reports the mass attenuation coefficient of the cadmium, and the two dashed lines represent the energies used for images acquisition. Values of the attenuation coefficients of the two base material used for the algorithm application are reported in table I.

As in previous case the flat-field correction has been applied on both images before processing.

4. – Results

4˙1. *First sample.* – Diffracted X-ray spectra acquired at different energies are reported in fig. 3. Results of measurements performed with the first sample are reported in fig. 4. At the top are reported normalized diffracted X-ray beams at energies of 25 keV, 26.7 keV, 27.4 keV and 28 keV and the mass attenuation coefficient of cadmium. In the middle panels are reported images of the cadmium sheet corrected for the flat field. In the bottom panels image profiles acquired in a ROI (Region Of Interest) of the images are shown. Dashed lines represent the position of the cadmium K-edge on the diffracted beam spectrum, on the image and on the profile. By increasing the energy the K-edge line shifts toward the left part of the image up to disappearing at 28 keV.

4˙2. *Second sample*. – In fig. 5 the low- and high-energy images acquired at 25 keV (a) and 28 keV (b) corrected for the flat field, used for the application of dual-energy technique, are reported. By comparing the two initial images one can see the presence of the K-edge energy represented by the dark region in the middle of the high-energy image. Figure 6a is the map of the cadmium distribution, while fig. 6b shows the distribution of the other materials, as established by eqs. (5) and (6). The map of cadmium and the distribution of the other materials is visible just in the middle region of the image in correspondence of which the two spectra are below and above the K-edge energy. Due to the the non-uniform distribution of the pigment in the cadmium image, cadmium granules are visible. Left and right regions of the images correspond to part of spectra both below or both above the K-edge. In these regions the algorithm does not provide significant results, due to the small difference of the cadmium attenuation coefficient.

5. – Conclusions and future developments

Preliminary tests have pointed out the possibility of using the K-edge method to investigate on the presence of a specific element in a painting layer. In particular the application of the dual-energy technique may obtain the planar distribution of the pigment. At the moment images size are about 15×3 cm^2. A scan system will soon be in use. In addition, to reduce the energy spread for a given image, the system will operate with two quasi-monochromatic beams obtained by a double-slit collimator and two linear digital detectors to simultaneously acquire the high- and low-energy images.

REFERENCES

[1] Bernasconi M., Cambria R., Dal Poz L., Del Carmine P., Grange M., Lucarelli F., Macarthur J. D. and Mandò P. A., *Analyse des couleurs dans un groupe de manuscrits enlumines du XII au XV siecle avec l'emploi de la technique PIXE*, in *Ancient and Medieval Book Materials and Techniques*, edited by Maniaci M. and Munafò P. F. (Biblioteca Apostolica Vaticana) 1993, pp. 357-358.
[2] Gigante G. E., Maltese C., Rinaldi S. and Sciuti S., *In situ ND analyses of XVI and XVII centuries Italian paintings*, in *Proceedings of Heidelberg International Conference "Archaeometry 90"*, edited by Pernicka E. and Wagner G. A. (1991).
[3] Milazzo M. and Cicardi C., *Archaeometry*, **40** (1998) 351.
[4] Mandò P. A., Fedi M. E., Grassi N. and Migliori A., *Nucl. Instrum. Methods B*, **239** (2005) 71.
[5] AA VV., *Art and Autoradiography: insights into the genesis od paintings by Rembrandt, Van Dick and Vermeer* (Metropolitan museum of Art, New York) 1987, pp. 9-18.
[6] Elleaume H. *et al.*, *Phys. Med. Biol.*, **45** (2000) 39.
[7] Dabin Y. *et al.*, *Nucl. Instrum. Methods A*, **467** (2001) 1342.
[8] Lehmann L. A. and Macovski A. *et al.*, *Med. Phys.*, **8** (1981) 659.
[9] Freund A. K., *Nucl. Instrum. Methods A*, **266** (1988) 461.
[10] Baldelli P. *et al.*, *Phys. Med. Biol.*, **50** (2005) 2225.
[11] Radeye2 Data Sheet (Rad-icon Imaging Corp.).
[12] Tuffanelli A. *et al*, *Nucl. Instrum. Methods A*, **489** (2002) 509.
[13] Sarnelli A. *et al*, *Phys. Med. Biol.*, **49** (2004) 3291.
[14] Berger M. J. and Hubbell J. H., *Photon Cross Sections on a Personal Computer*, in NBSIR 87-3597 (National Institute of Standards and Technology, Gaithersburg, MD).